Chain Link Deformation in the Nonlinear Dynamics of Tracked Vehicles

M. K. SARWAR
TOSHIKAZU NAKANISHI
A. A. SHABANA
Department of Mechanical Engineering, University of Illinois at Chicago, P.O. Box 4348, Chicago, IL 60680, U.S.A.

(Received 19 January 1994, accepted 6 March 1995)

Abstract: In this investigation, a computational finite element procedure for the deformation and stress analysis of the chain links of tracked vehicles is presented and used to examine the validity of using the static approach in the design and stress analysis of tracked vehicles. The contact forces resulting from the interaction between the track links and the vehicle components (sprocket, idler, and the rollers) as well as the interaction between the track links and the ground are evaluated using continuous force models, which are used to define generalized contact forces associated with the deformation degrees of freedom of the track links using the virtual work. The dynamic forces including the contact forces used in the finite element procedure developed in this investigation are evaluated using a 54-body vehicle model in which the track is modeled as a closed kinematic chain with 42 degrees of freedom. It is demonstrated in this study that the effect of the contact forces is more significant as compared to the effect of the rigid-body inertia forces of the chain links, and consequently, it is assumed that the deformation of the track links does not have a significant effect on the overall motion of the vehicle. In the finite element computational procedure used in this study, three-dimensional solid elements are used to discretize the links of the track chain. The numerical results presented in this investigation demonstrate that the use of the static analysis may lead to low estimates of the stresses of the track links as compared to those obtained by a dynamic stress analysis that takes into consideration the time history of the forces.

Key Words: Tracked vehicles, chain links, multibody dynamics, finite element stress analysis, track deformation

1. INTRODUCTION

Due to the substantial computational capabilities required for the dynamic analysis of large-scale multibody tracked vehicle systems, simple models have been used to study the track links and sprocket interaction. These simplified models, however, are not adequate to describe the complex nature of interaction between the tracked vehicle components. In heavy-load vehicles such as bulldozers, hydraulic excavators, and other earthmoving equipment, the track links are subjected to large contact forces as the result of their interaction with the rollers, the idler, and the sprocket of the vehicle as well as with the ground. These forces, in addition to increasing the vibration and noise level, produce high stress levels that cause damage to the track links and the vehicle components. Quite often, for the sake of simplicity, the deformations of the track links are examined using static-force analysis. The purpose of this study is to demonstrate the errors that may result from the use of static-force analysis in the study of the deformation of the track links. The

Journal of Vibration and Control 1: 201–224, 1995

contribution and effect of each dynamic force such as the contact, inertia, centrifugal, and joint forces are examined and quantified.

Naji and Marshek (1983) conducted an experimental study to determine the effect of elastic properties, geometric variations, and lubrication on the roller-chain load distribution. The load distribution was found for a large number of cases to be independent of the elastic properties of the chain and the sprocket. It was also found that the two lubricants used in the experiment had no noticeable effect on the load distribution. In the case of the pitch difference between the chain links and the sprocket teeth, it was found that a larger pitch of the sprocket tooth amplifies the tension in the chain link. Naji and Marshek (1984) examined the effect of the pitch difference on the roller-chain articulation angles and pressure angles. The tooth surface assumed to consist of four portions: seating curve, working curve, straight portion, and topping curve. Strategies were given for locating the contact points, and the results obtained were compared with the graphical solution. It was found that, due to the pitch difference between the sprocket teeth and the chain links, the pressure angles and the chain articulation angles of the engaged roller vary from roller to roller. It was also found that a sprocket with a fewer number of teeth can accommodate a higher percentage pitch difference without jumpage. Naji and Marshek (1984) pointed out that in cases where the pitch difference is due to wear-elongation of the chain, the contact points and, consequently, the pressure angles and the chain articulation angles each converge to two distinct values. These two values are only a function of the pitch difference.

Chew (1985) represented the shock load due to the roller-sprocket impact in a chain drive by an effective mass, which is the mass observed at the point and instant of impact. This mass is a function of the total number of links in the chain span and the mass distribution within a chain link. Chew (1985) found that the effective mass of the chain decreases with increase in the chain length. Furthermore, the impulsive force on the links in the chain span decreases exponentially with the distance from the impacted roller.

Veikos and Freudenstein (1992) developed a computer procedure for the dynamic analysis of roller-chain drives. Important factors of chain dynamics such as impact, discontinuities in span length, chain elasticity, coupling between longitudinal and transverse motion, and coupling between the motion and boundary conditions were considered. The procedure developed by Veikos and Freudenstein (1992) was used to study various chain configurations. The results obtained showed good agreement with experimental observations. Bucknor and Freudenstein (1992) developed a quasi-static model for a silent (inverted tooth) chain drive featuring a rocker-pin-jointed chain and sprockets with involute teeth. The model takes into account the effects of clearances in the rocker-pin joints and the geometry of the link-sprocket engagement. The effect of the fluctuations in the torque-ratio due to chordal action was examined. An optimization method was also developed and used as an aid in determining the governing geometric constraints because multiple-joint configurations can be selected.

Bando, Yoshida, and Hori (1991) outlined the design and development of rubber-tracked small-size bulldozers. Computer-simulation results of the vehicle were presented, and the vehicle performance was evaluated. Simulation results indicate that the vehicle has favorable characteristics, such as less damage to road surfaces, and reduced vibration and noise.

McCullough and Haug (1985) presented the concept of superelement that represents the dynamics of high-mobility track-vehicle suspension systems. All the parts of the suspension, including the track, sprocket, and all the rollers, wheels, and roller arms, were defined as superelements. The equations of motion for the subsystems were derived using a variational form of the rigid-body equations of motion. The analysis, however, was limited to modeling kinematic effects of the track, neglecting the track-loop rotational degrees of freedom and vibration modes. The track was represented as an internal-force element, and a relaxed catenary relationship was used to compute the track tension. In modeling the soil-track interface, empirical normal and shear force formulas based on constitutive relations of soil mechanics were used.

Murray and Canfield (1992) modeled the track link and sprocket system of a tracked vehicle using supercomputers. A general-purpose three-dimensional multi-rigid-body computer program was used, and the behavior of the interaction of the track link and sprocket was illustrated graphically. It was found that the use of supercomputers saves hundreds of hours of computer time when the track-sprocket interaction is analyzed.

Nakanishi and Shabana (1992, 1994) presented a method for the computer-aided dynamic analysis of large-scale tracked vehicles. The track of the vehicle that consists of a large number of rigid links connected by revolute joints was modeled as a closed kinematic chain. The impacts between the ground and the track links, and between the track links and the rollers, the idler, and the sprocket, were described using a continuous contact-force model (Khulief and Shabana, 1987). The stiffness and damping coefficients in the force model were determined by studying the vibration characteristics of the vehicle. The Lagrangian formulation was used to develop the dynamic equations of motion of the tracked vehicle, and the coordinate partitioning of the constraint Jacobian matrix was employed in order to identify a set of independent coordinates. The associated independent-state equations were integrated numerically in order to determine the independent coordinates and velocities. An iterative Newton-Raphson algorithm was used to determine the dependent coordinates and velocities using the nonlinear kinematic constraint relationship.

In tracked vehicles, the track links are subjected to high contact forces that produce high stress levels, which often cause damage to the track links during the functional operation of the vehicle. Surprisingly, despite the widespread use of tracked vehicles in civilian and military applications, little has been published about their basic mechanics including the study of the track link deformation. This is mainly due to the complexity of the problem, which requires sophisticated numerical and computer methods to solve the resulting system of nonlinear differential and algebraic equations of the tracked vehicles. Stresses and wear of the track links are often examined using static-load analysis. It is, therefore, the objective of this investigation to develop a computer-aided dynamic-analysis procedure that can be used to study the track-link deformation and clearly demonstrate the discrepancy and errors that result from the use of static-force analysis of the track links. In the procedure presented in this paper, the equations of motion of the vehicle developed using the principle of virtual work in dynamics are expressed in terms of a coupled set of reference and elastic coordinates.

Continuous contact-force models are used to describe the contact between the track links and the rollers, the sprocket, the idler, and the ground. The equations of motion

are simplified by assuming that the deformation of the steel track links does not have a significant effect on the overall rigid-body displacement of the vehicle. The forces that act on the track links as the result of their interaction with the ground and the vehicle components are analyzed, and the inertia, Coriolis, and centrifugal forces as well as the constraint and contact forces acting on the track links are examined. These forces are used in this paper in a computational finite element procedure in order to study the deformation and dynamic stresses of the track links as the result of their interaction with the vehicle component as well as the ground. The results obtained from the dynamic stress analysis are compared with the results of the static force analysis in order to demonstrate the discrepancies and errors that arise from neglecting the dynamic effects in the analysis of the track-link deformations.

2. TRACKED VEHICLE MODEL

The vehicle model used in this study is shown in Figure 1a, while the planar model, which consists of 54 bodies and is used in the numerical study presented in this paper, is shown in Figure 1b (Nakanishi and Shabana, 1992, 1994). Ground is denoted as body 1, the chassis as body 2, the driving sprocket as body 3, and the idler as body 4. Bodies 5 to 11 are the lower rollers, body 12 is the upper roller, and bodies 13 to 54 are the track links. The track links are connected to each other by revolute joints forming a closed kinematic chain that has 42 degrees of freedom, and the rollers, the idler, and the sprocket are connected to the chassis of the vehicle by revolute joints. The total number of degrees of freedom of the tracked vehicle is 54. The driving sprocket of the vehicle has 21 teeth, and its pitch circle diameter is 0.594 m. The chain pitch P_c is assumed to be double the sprocket tooth pitch P_s, which is equal to 0.0875 m.

The contact forces between the rollers and the track links, the sprocket and the track links, the idler and the track links, and the ground and the track links are evaluated

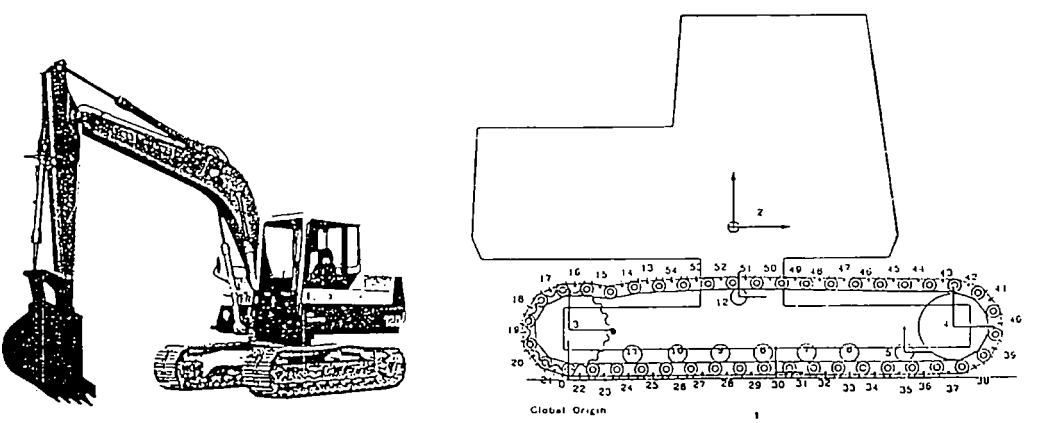

(a) (b)

Figure 1. Tracked vehicle model.

by studying the vibration characteristics of the vehicle. The contact force depends on the material of the track links, the speed of the moving parts, friction, and so forth. The method used to calculate the contact forces (Nakanishi and Shabana, 1992, 1994) is based on the principle that the equivalent spring coefficient of two springs connected in series is equal to or less than the lowest stiffness coefficient of the spring. To obtain the equivalent stiffness coefficient, the vehicle natural frequencies of oscillation were measured experimentally.

A continuous contact force model is used to represent the interaction between the track links and the sprocket, the idler, and the rollers as well as the ground. The contact force model used in this investigation is defined as

$$F_c^{ij} = k\delta^{ij} + c\dot{\delta}^{ij} \tag{1}$$

where F_c^{ij} is the contact force between body i and body j, k and c are, respectively, the stiffness and damping coefficients, and δ^{ij} is the penetration of the surfaces in contact. To define the contact force between the sprocket teeth and track links, a simplified tooth profile in which the tooth surface is described by three surfaces is used. A local coordinate system is rigidly attached to each surface (Nakanishi and Shabana, 1992, 1994), and the orientations of these coordinate systems with respect to the sprocket coordinate system are defined using constant transformations matrices. The surface coordinate systems are used to define the location of the track pins with respect to the teeth of the sprocket. A similar, but simpler, procedure is used to define the locations of the track links with respect to the ground and with respect to the rollers and the idler of the vehicles.

Dynamic Model

The equations of motion of the deformable body i in the tracked vehicle model can be obtained using the principle of virtual work, which is stated as

$$\delta W_i^i = \delta W_s^i + \delta W_e^i + \delta W_c^i \tag{2}$$

where δW_i^i is the virtual work of the inertia forces, δW_s^i is the virtual work of the elastic forces resulting from the body deformation, δW_e^i is the virtual work of the externally applied forces, and δW_c^i is the virtual work of the constraint forces. The principle of virtual work leads to the following system of equations of motion for the deformable body i (Shabana, 1989, 1994),

$$\mathbf{M}^i\ddot{\mathbf{q}}^i + \mathbf{K}^i\mathbf{q}^i + \mathbf{C}_{\mathbf{q}^i}^{\mathrm{T}}\boldsymbol{\lambda} = \mathbf{Q}_e^i + \mathbf{Q}_v^i \tag{3}$$

where $\mathbf{M}^i$ and $\mathbf{K}^i$ are, respectively, the symmetric mass and stiffness matrices, $\mathbf{q}^i$ is the vector of generalized coordinates, $\mathbf{Q}_e^i$ is the vector of externally applied and contact forces, $\mathbf{Q}_v^i$ is the vector of centrifugal and Coriolis inertia forces, $\boldsymbol{\lambda}$ is the vector of Lagrange multipliers, $\mathbf{C}(\mathbf{q}, t)$ is the vector of kinematic constraint equations that describe the revolute joints in the tracked vehicle model, and $\mathbf{C}_{\mathbf{q}^i}$ is the constraint Jacobian matrix that is obtained by differentiating the vector of constraint equations with respect to the vector

of generalized coordinates $\mathbf{q}^i$. Equation (3) can be written in the following partitioned form (Shabana, 1989)

$$\begin{bmatrix} \mathbf{m}^i_{rr} & \mathbf{m}^i_{rf} \\ \mathbf{m}^i_{fr} & \mathbf{m}^i_{ff} \end{bmatrix} \begin{bmatrix} \ddot{\mathbf{q}}^i_r \\ \ddot{\mathbf{q}}^i_f \end{bmatrix} + \begin{bmatrix} \mathbf{0} & \mathbf{0} \\ \mathbf{0} & \mathbf{K}^i_{ff} \end{bmatrix} \begin{bmatrix} \mathbf{q}^i_r \\ \mathbf{q}^i_f \end{bmatrix} + \begin{bmatrix} \mathbf{C}^{\mathrm{T}}_{\mathbf{q}^i_r} \\ \mathbf{C}^{\mathrm{T}}_{\mathbf{q}^i_f} \end{bmatrix} \boldsymbol{\lambda} = \begin{bmatrix} \left(\mathbf{Q}^i_e\right)_r \\ \left(\mathbf{Q}^i_e\right)_f \end{bmatrix} + \begin{bmatrix} \left(\mathbf{Q}^i_v\right)_r \\ \left(\mathbf{Q}^i_e\right)_f \end{bmatrix} \tag{4}$$

where subscripts r and f refer, respectively, to reference and elastic coordinates.

Flexibility of the Track Links

Because of the contact forces between the track links and rollers, sprocket, and ground, the steel track links are subjected to high impulsive forces, which significantly increase the vibration and noise and produce a high level of dynamic stresses. The compressive contact forces in addition to the tensile driving forces have significant effects on the track dynamics. It is assumed in the analysis presented in this study that the steel track deformation does not have a significant effect on the overall dynamic motion of the tracked vehicle. If the effect of small deformation on the rigid-body motion of the track links is neglected, equation (4) yields the following two equations

$$\mathbf{m}^i_{rr}\ddot{\mathbf{q}}^i_r + \mathbf{C}^{\mathrm{T}}_{\mathbf{q}^i_r}\boldsymbol{\lambda} = \left(\mathbf{Q}^i_e\right)_r + \left(\mathbf{Q}^i_v\right)_r \tag{5}$$

and

$$\mathbf{m}^i_{ff}\ddot{\mathbf{q}}^i_f + \mathbf{K}^i_{ff}\mathbf{q}^i_f = \left(\mathbf{Q}^i_e\right)_f + \left(\mathbf{Q}^i_v\right)_f - \mathbf{C}^{\mathrm{T}}_{\mathbf{q}^i_f}\boldsymbol{\lambda} - \mathbf{m}^i_{fr}\ddot{\mathbf{q}}^i_r. \tag{6}$$

In equation (5), the effect of the deformation on the rigid-body dynamics of the track links is neglected. Equation (6), on the other hand, governs the elastic vibrations of the track links. In this equation, the effect of the rigid-body motion on the elastic deformation is taken into consideration. Equation (5) can be solved using the method of rigid-body dynamic analysis in order to determine the rigid-body inertia forces and the joint reaction forces. These forces, as demonstrated in later sections, are used to solve for the elastic deformation of the track links.

Rigid-Body Simulation

The dynamics of the tracked vehicle that consists of interconnected rigid bodies is governed by a set of equations in the form of equation (5). If a centroidal body coordinate system is used, the vector $(\mathbf{Q}^i_v)_r$ is identically zero, and the mass matrix $\mathbf{m}^i_{rr}$ is diagonal. In this case, the dynamic equations that describe the rigid-body motion of the tracked vehicle can be written as

$$\mathbf{m}^i_{rr}\ddot{\mathbf{q}}^i_r + \mathbf{C}^{\mathrm{T}}_{\mathbf{q}^i_r}\boldsymbol{\lambda} = \left(\mathbf{Q}^i_e\right)_r \qquad i = 1, 2, \ldots, n_b \tag{7}$$

where $n_b = 54$ is the total number of bodies in the vehicle. The preceding equation can also be written as

$$\mathbf{M}_{rr}\ddot{\mathbf{q}}_r + \mathbf{C}^{\mathrm{T}}_{\mathbf{q}_r}\boldsymbol{\lambda} = (\mathbf{Q}_e)_r \tag{8}$$

where $\mathbf{M}_{rr}$ is the system mass matrix, $\mathbf{C}_{\mathbf{q}_r}$ is the Jacobian matrix of the kinematic constraints, and $(\mathbf{Q}_e)_r$ is the vector of generalized external forces. The dimension of the vector $\mathbf{q}_r$ for the vehicle model shown in Figure 1b is 162.

The constraint equations that describe the revolute joints as well as the specified motion trajectory of the sprocket can be written as

$$\mathbf{C}(\mathbf{q}_r, t) = \mathbf{0}. \tag{9}$$

Differentiating the kinematic constraint relationships of equation (9) twice with respect to time, one obtains

$$\mathbf{C}_{\mathbf{q}_r}\ddot{\mathbf{q}}_r = \mathbf{Q}_d \tag{10}$$

where $\mathbf{Q}_d$ is a vector that absorbs terms that are quadratic in the velocities. Equations (8) and (10) can be combined yielding

$$\begin{bmatrix} \mathbf{M}_{rr} & \mathbf{C}_{\mathbf{q}_r}^{\mathrm{T}} \\ \mathbf{C}_{\mathbf{q}_r} & \mathbf{0} \end{bmatrix} \begin{bmatrix} \ddot{\mathbf{q}}_r \\ \boldsymbol{\lambda} \end{bmatrix} = \begin{bmatrix} (\mathbf{Q}_e)_r \\ \mathbf{Q}_d \end{bmatrix}. \tag{11}$$

This equation can be solved for the accelerations and the vector of Lagrange multipliers. The accelerations can be integrated forward in time to determine the coordinates and velocities. A predictor-corrector numerical integration method coupled with an iterative Newton-Raphson scheme is used to obtain the state of the system and check on the violation of the kinematic constraints (Wehage, 1980; Shabana, 1994). Figure 2 shows the vertical and horizontal displacements of the track link number 13 as a function of time. The results presented in the two parts of this figure can be used to define the trajectories of the track links, which are shown in the computer animation of the motion of the tracked vehicle shown in Figure 3.

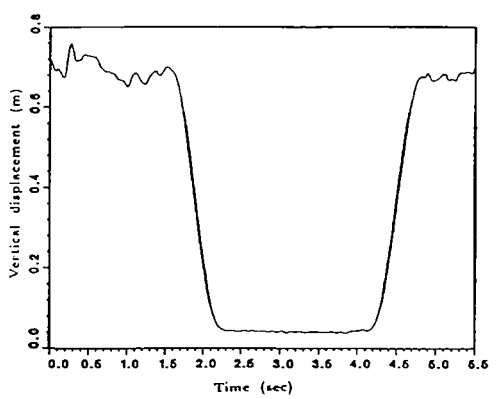

(a) Vertical displacement

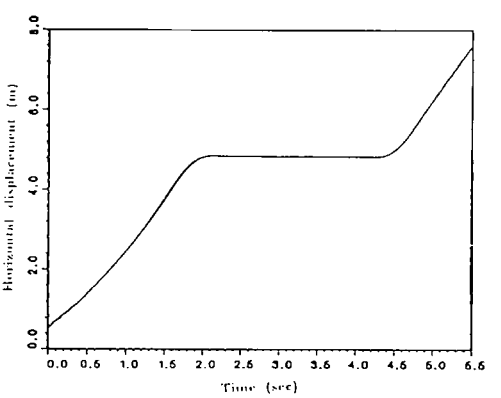

(b) Horizontal displacement

Figure 2. Motion of the track link 13.

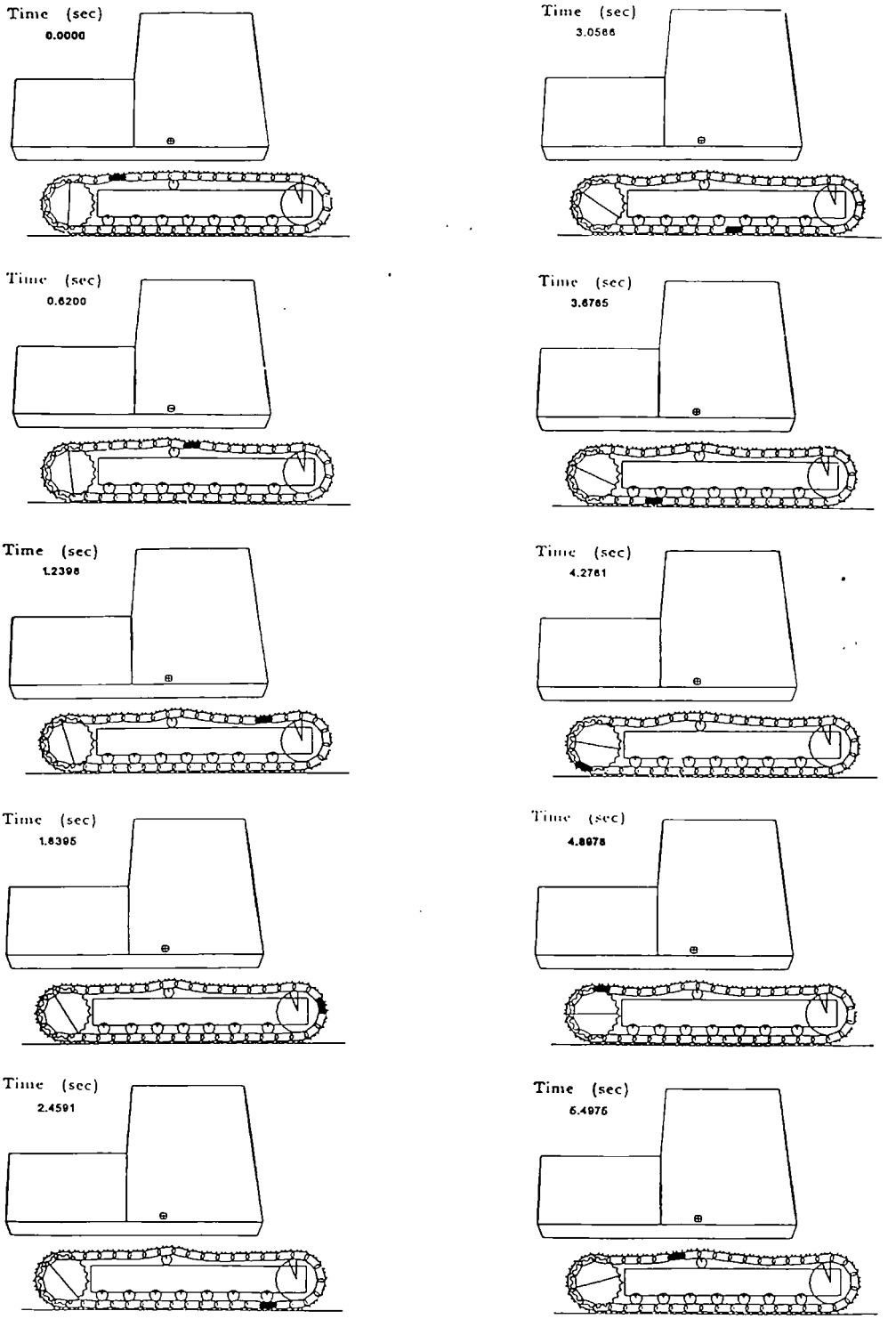

Figure 3. Computer animation of the tracked vehicle.

3. JOINT FORCES

The solution of equation (11) defines the vector of Lagrange multipliers, which can be used to determine the generalized joint reaction forces associated with the generalized reference coordinates. Let $\boldsymbol{\lambda}_k$ be the vector of Lagrange multipliers associated with the vector $\mathbf{C}_k$ that describes the constraints of the revolute joint between the track links i and j. The generalized reaction forces of the revolute joint k acting on the track link i can then be written as

$$\mathbf{F}_k^i = -(\mathbf{C}_k)_{\mathbf{q}^i}^{\mathrm{T}} \boldsymbol{\lambda}_k = -\mathbf{F}_k^j \tag{12}$$

where $\mathbf{F}_k^j$ is the vector of generalized reaction forces acting on link j as the result of its connection with link i. The numerical values of the vector $\mathbf{F}_k^i$ and $\mathbf{F}_k^j$ are readily available from the dynamic simulation. The tension and the compression forces acting on the track links can be obtained by determining the reaction forces acting at the joint definition points. To this end, the virtual work is used to obtain a system equipollent to the system of forces defined by equation (12). The generalized forces $\mathbf{F}_k^i$ can be written as

$$\mathbf{F}_k^i = \left[\mathbf{F}_{kR}^{i^{\mathrm{T}}} \;\; F_{k\theta}^i\right]^{\mathrm{T}} \tag{13}$$

where $\mathbf{F}_{kR}^i$ and $F_{k\theta}^i$ are the generalized reaction forces associated with the translation and rotation of the coordinate system of the track link i. Using the virtual work, it can be shown that

$$\mathbf{F}_{kR}^i = -\begin{bmatrix} \lambda_{k_1} \\ \lambda_{k_2} \end{bmatrix} \tag{14}$$

where λ_{k_1} and λ_{k_2} are the Lagrange multipliers associated with the constraint equations of the revolute joint k. Figure 4 shows the horizontal and vertical components of the reaction forces at the joint that connects the track links 13 and 54 as a function of time.

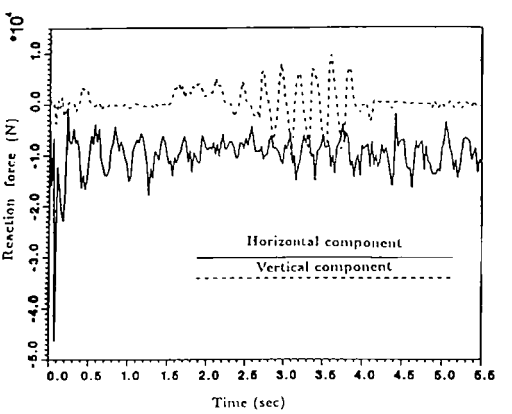

Figure 4. Horizontal and vertical components of the joint force between bodies 13 and 54.

These reaction forces are defined in the coordinate system of the track link 13. It is clear from the results presented in this figure that the vertical component of the reaction force significantly increases when the track link is in contact with the ground and the seven lower rollers.

In flexible body dynamics, the generalized joint reaction forces associated with the elastic coordinates do not represent independent variables. They can be calculated once the joint forces associated with the reference motion are determined. Chen, Shabana, and Rismantab-Sany (1991) obtained the following relationship between the constraint Jacobian matrices associated with the reference and elastic coordinates

$$\mathbf{C}_{\mathbf{q}_f^i} = \mathbf{C}_{\mathbf{R}^i}\mathbf{A}^i\mathbf{S}_P^i \tag{15}$$

where $\mathbf{A}^i$ is the planar transformation matrix that defines the orientation of link i, and $\mathbf{S}_P^i$ is the shape function of the link i defined at the joint definition point. Equation (15) implies that, if the assumed displacement field of the link i is defined, the constraint Jacobian matrix $\mathbf{C}_{\mathbf{q}_f^i}$ associated with the elastic coordinates can be determined if the Jacobian matrix $\mathbf{C}_{\mathbf{R}^i}$ associated with the reference translation and the transformation matrix $\mathbf{A}^i$ are evaluated. Equation (15) can be used to determine the generalized joint forces associated with the elastic coordinates of the track links. These generalized reaction forces, which appear in equation (6), can be written as

$$\mathbf{C}_{\mathbf{q}_f^i}^{\mathrm{T}}\boldsymbol{\lambda} = \mathbf{S}_P^{i^{\mathrm{T}}}\mathbf{A}^{i^{\mathrm{T}}}\mathbf{C}_{\mathbf{R}^i}^{\mathrm{T}}\boldsymbol{\lambda}. \tag{16}$$

These generalized reaction forces associated with the elastic degrees of freedom of the track links will be used to study the link deformation in the section entitled Track Link Deformation Model.

4. CENTRIFUGAL AND CORIOLIS INERTIA FORCES

It is clear from equation (6) that the effect of the rigid-body inertia on the elastic deformation of the track links is represented by the vector

$$\mathbf{F}_i^i = -\mathbf{m}_{fr}^i\ddot{\mathbf{q}}_r^i = -\begin{bmatrix}\mathbf{m}_{fR}^i & \mathbf{m}_{f\theta}^i\end{bmatrix}\begin{bmatrix}\ddot{\mathbf{R}}^i \\ \ddot{\theta}^i\end{bmatrix} \tag{17}$$

where the matrix $\mathbf{m}_{fr}^i$ is defined as (Shabana, 1989)

$$\mathbf{m}_{fr}^i = \begin{bmatrix}\overline{\mathbf{S}}^{i^{\mathrm{T}}}\mathbf{A}^{i^{\mathrm{T}}} & \mathbf{m}_{f\theta}^i\end{bmatrix} \tag{18}$$

and

$$\left.\begin{aligned}\overline{\mathbf{S}}^i &= \int_{V^i}\rho^i\mathbf{S}^i\,dV^i \\ \mathbf{m}_{f\theta}^i &= \int_{V^i}\rho^i\mathbf{S}^{i^{\mathrm{T}}}\tilde{\mathbf{I}}^{\mathrm{T}}\overline{\mathbf{u}}^i\,dV^i\end{aligned}\right\} \tag{19}$$

in which $\mathbf{S}^i$ is the shape function of the track link i, ρ^i and V^i are, respectively, the mass density and volume of the link, $\bar{\mathbf{u}}^i$ is the local position vector of an arbitrary point on the link, and $\tilde{\mathbf{I}}$ is the skew symmetric matrix

$$\tilde{\mathbf{I}} = \begin{bmatrix} 0 & 1 \\ -1 & 0 \end{bmatrix}.$$

Figures 5 and 6 show the components of the acceleration of the track link 13 during a complete cycle. It is clear from the results presented in these figures that the angular acceleration significantly decreases when the track link is in contact with the ground and the lower rollers.

The vector $(\mathbf{Q}_v^i)_f$ of the Coriolis and centrifugal forces that appear in equation (6) can be written as (Shabana, 1989)

$$\left(\mathbf{Q}_v^i\right)_f = (\dot{\theta}^i)^2\left(\mathbf{m}_{ff}^i\mathbf{q}_f^i + \bar{\mathbf{I}}_0^i\right) + 2\dot{\theta}^i\tilde{\mathbf{S}}^i\dot{\mathbf{q}}_f^i \tag{20}$$

where $\tilde{\mathbf{S}}^i$ is the skew symmetric matrix

$$\tilde{\mathbf{S}}^i = \int_{V^i} \rho^i \mathbf{S}^{iT}\tilde{\mathbf{I}}\mathbf{S}^i\, dV^i$$

and

$$\bar{\mathbf{I}}_0^i = \int_{V^i} \rho^i \mathbf{S}^{iT}\bar{\mathbf{u}}_0^i\, dV^i \tag{21}$$

where $\bar{\mathbf{u}}_0^i$ is the position vector of an arbitrary point of the track link in the undeformed state. If the deformation of the track link is assumed to be small, the vector $(\mathbf{Q}_v^i)_f$ of the

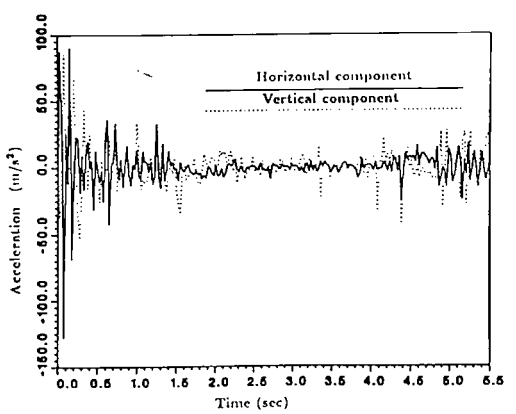

Figure 5. Horizontal and vertical components of the acceleration of the track link 13.

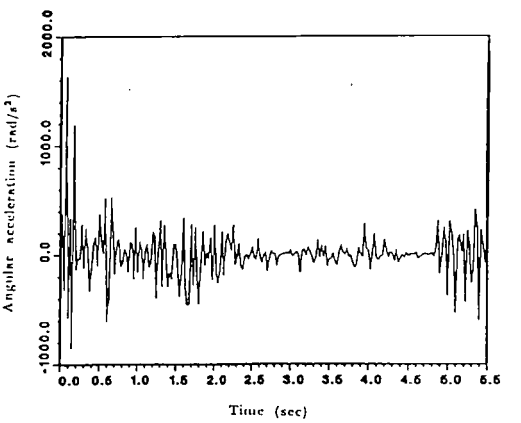

Figure 6. Angular acceleration of the track link 13.

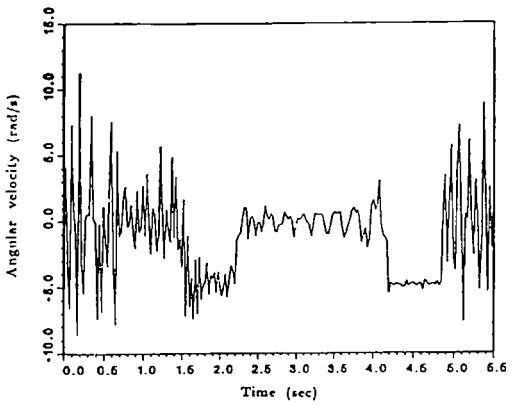

Figure 7. Angular velocity of the track link 13.

Coriolis and centrifugal forces can be approximated as

$$\left(\mathbf{Q}_v^i\right)_f = (\dot{\theta}^i)^2\, \bar{\mathbf{I}}_0^i. \tag{22}$$

It is clear from this equation that the centrifugal force vector $(\mathbf{Q}_v^i)_f$ is a quadratic function of the angular velocity of the track link. Figure 7 shows the angular velocity of the track link 13 as a function of time. It is clear from the results presented in this figure that the angular velocity of the track link is relatively small when the track link is in contact with the ground. Equation (22) can be used to determine the centrifugal forces associated with the elastic coordinates of the track link if the angular velocity $\dot{\theta}^i$ is determined from a rigid-body simulation.

5. CONTACT FORCES

The analysis of the contact forces is one of the most difficult tasks in the study of the nonlinear dynamics of large-scale tracked vehicles. These forces, which are the result of the interaction between the track links and the sprocket, the idler, the rollers, and the ground, have a significant effect on the deformation of the track links as well as on the dynamic behavior of the vehicle.

Sprocket Track Interaction

In the course of the engagement between the sprocket teeth and the track links, several sprocket teeth can be in contact with several track links at the same time. As shown in Figure 8, there are four possibilities that may occur regarding the contact between a sprocket tooth and a track link pin. In the first case, there is no contact between the track link pin and the sprocket tooth; in the second case, the track link pin comes into contact with the *left surface* **e** of the sprocket tooth; in the third case, the track link pin comes into contact with the *seating surface* **b** of the sprocket tooth; and in the fourth case, the track link pin comes into contact with the *right surface* **g** of the sprocket tooth. To describe the contact between a track link pin and a sprocket tooth, three coordinate

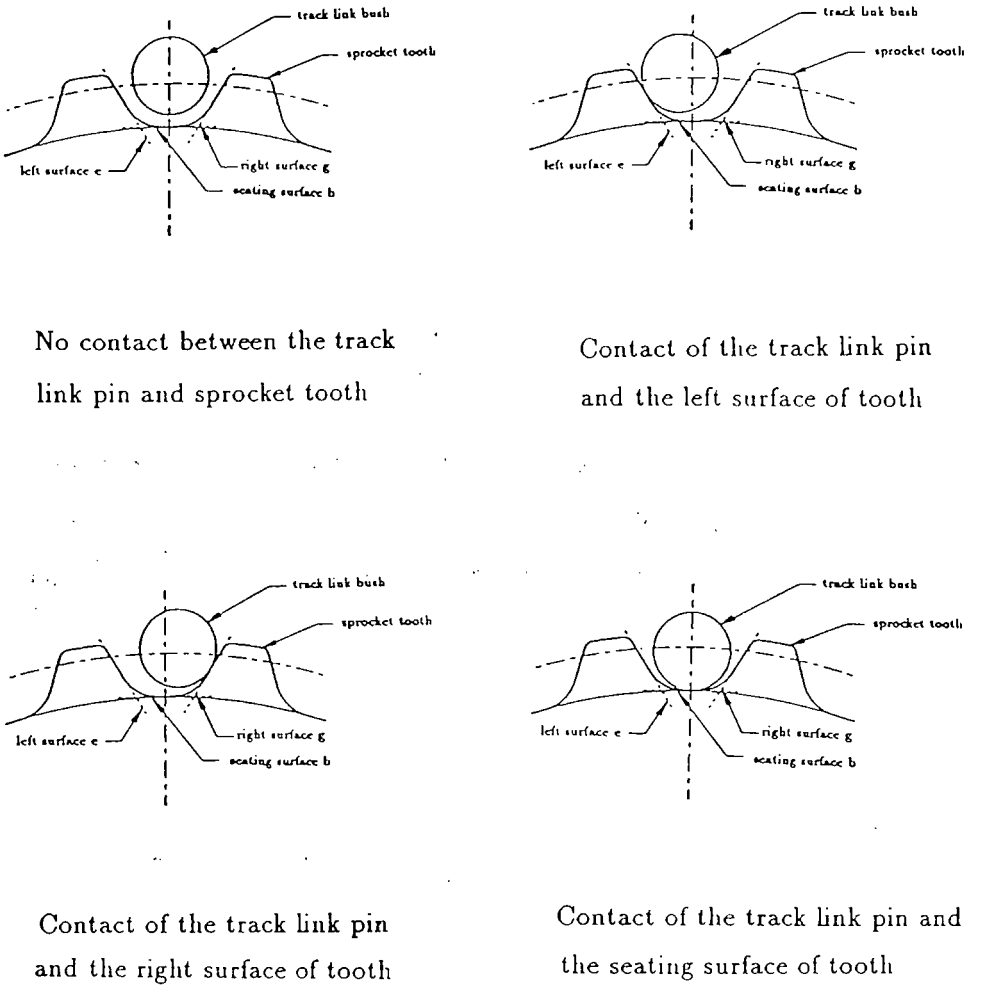

Figure 8. Contact between the track link pin and the sprocket tooth surfaces.

systems are introduced for each tooth surface as described in Nakanishi and Shabana (1992, 1994). In addition to these three coordinate systems, a tooth coordinate system is also introduced. These four coordinate systems, in addition to the sprocket coordinate system and the track-link coordinate systems, are used to define the time and points of contact (Nakanishi and Shabana, 1992, 1994). A continuous force model as described by equation (1) is used to define the contact forces between the sprocket teeth and the track links. By monitoring the global position vectors of the points on the surfaces of the track links and the sprocket teeth, the contacts can be predicted and the penetration δ^{ij} can be evaluated.

Figure 9 shows the normal component of the contact force acting on the track link 13 as the result of its engagement with the sprocket teeth. This force component is plotted versus time to show the contact periods. The stiffness and damping coefficients used in the contact force model are 5.0×10^6 N/m and 1.34×10^4 N·s/m, respectively.

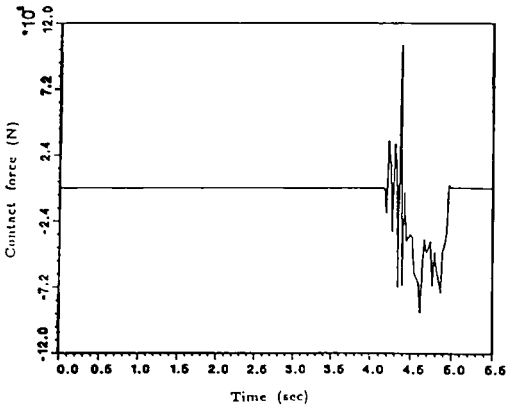

Figure 9. Normal contact force acting on the track link 13 as the result of the engagement with the sprocket.

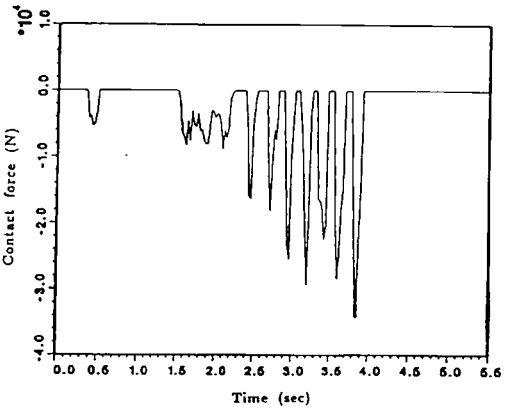

Figure 10. Normal force acting on the track link 13 as the result of the contact with the rollers and the idler.

Roller Track Interaction

To determine the conditions for the contact between the surfaces of the track links and the rollers and the idler, the global position vectors of the points on these surfaces are monitored to determine which surfaces are in contact (Nakanishi and Shabana, 1992, 1994). Continuous force models are also used to describe the impulsive forces resulting from the impact between the rollers and the idler and the track links. The stiffness and damping coefficients used in these continuous force models are 0.25×10^8 N/m and 1.52×10^4 N·s/m, respectively. Figure 10 shows the normal component of the force acting on the track link 13 as the result of its contact with the rollers and the idler.

Ground Track Interaction

Each track link in the vehicle model used in this investigation has a triple shoe plate. Consequently, a three-point contact-force model is used to calculate the contact forces between the ground and the track links. In this study, the ground is assumed to be a flat surface road and the friction between the track links and the ground is represented by a simple Coulomb friction model. The stiffness and damping coefficients used to describe the contact between the track link and the ground are 1.0×10^6 N/m and 6.1×10^3 N·s/m, respectively. The coefficient of Coulomb friction used in this investigation is 0.1. Figure 11 shows the contact forces, as a function of time, at the three contact points on the track link 13. These contact points are shown in Figure 12.

6. TRACK LINK DEFORMATION MODEL

The track of the vehicle model shown in Figure 1b consists of 42 links connected by revolute joints. Figure 12a shows the basic structure of the link. The track pitch length of a track link is considered as the distance between the centers of the two consecutive pin joints, which is equal in the model used in this investigation to 175 mm. The width of the track link is 500 mm, and the total length of the track link chain is 7.35 m. The assembly of a track link whose weight is 18.7 kg consists of one shoe plate, two tracks bolted to the

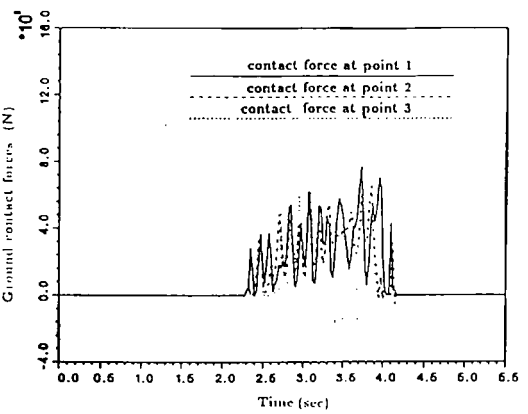

Figure 11. Normal contact forces acting on the track link 13 as the result of the contact with the ground.

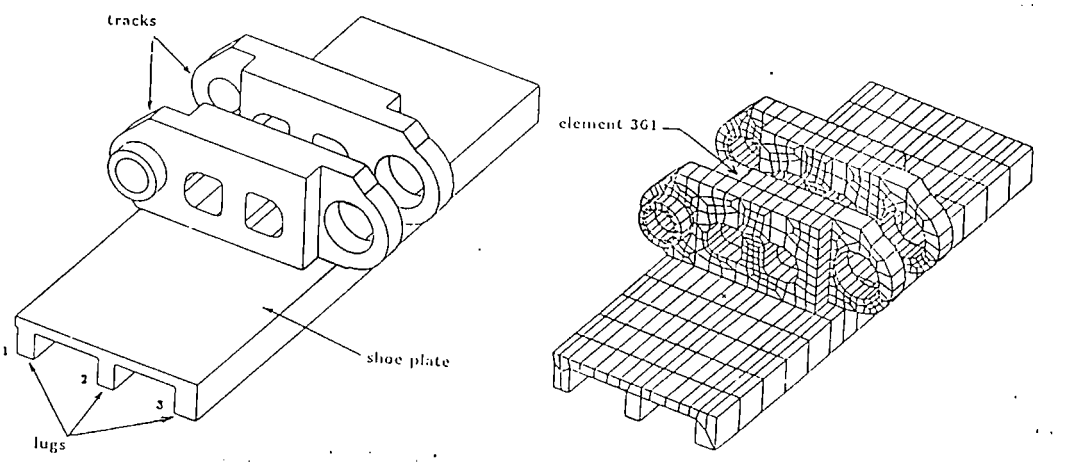

(a) Triple lugs track link (b) Finite element model

Figure 12. Structure and the finite element model of the track link.

shoe plate, bushing, and pin. The shoe plate, which has an overall length of 198.9 mm, has three lugs called graucers and named as triple shoe. The two ends of the shoe plate are not identical; one end curves upward in a tapered form and the other end bends down providing concave surface in a lob form. In an assembled form of the closed track chain, end portions of track shoe overlap each other, thereby protecting excess dirts and muds from entering into the upper parts of the plates. The tracks bolted to the shoe plate, which are case-hardened, are of the offset type that has higher carbon steel than the shoe plate. The revolute joints consisting of bushing and pin are driven by the driving sprocket of the excavator. During this process, the bushing that encloses the pin comes in contact with the surfaces of the sprocket teeth.

For a track link i, equation (6) can be written as

$$\mathbf{m}_{ff}^{i}\ddot{\mathbf{q}}_{f}^{i} + \mathbf{K}_{ff}^{i}\mathbf{q}_{f}^{i} = \mathbf{F}^{i}(t) \tag{23}$$

where

$$\mathbf{F}^i(t) = \left(\mathbf{Q}_e^i\right)_f + \left(\mathbf{Q}_v^i\right)_f - \mathbf{C}_{\mathbf{q}_f^i}^{\mathrm{T}} \boldsymbol{\lambda} - \mathbf{m}_{fr}^i \ddot{\mathbf{q}}_r^i \tag{24}$$

Utilizing the fact that $\mathbf{m}_{ff}^i$ and $\mathbf{K}_{ff}^i$ are constant, and can be evaluated using the finite element method, component mode synthesis can be used to obtain a set of uncoupled ordinary differential equations for each link. In this approach, the following orthogonality conditions hold (Burnett, 1987; Shabana, 1991)

$$\boldsymbol{\Phi}_k^{i^T} \mathbf{K}_{ff}^i \boldsymbol{\Phi}_l^i = \omega_k^2 \delta_{kl} \tag{25}$$

and

$$\boldsymbol{\Phi}_k^{i^T} \mathbf{m}_{ff}^i \boldsymbol{\Phi}_l^i = \delta_{kl} \tag{26}$$

where

$$\delta_{kl} = 1 \quad \text{if} \quad k = l$$

$$\delta_{kl} = 0 \quad \text{if} \quad k \neq l$$

and $\boldsymbol{\Phi}_k^i$ is the eigenvector associated with mode k.

Using the orthogonality conditions of equations (25) and (26), one obtains the following set of uncoupled differential equations expressed in terms of the modal coordinates

$$\ddot{P}_k^i + (\omega_k)^2 P_k^i = Q_k^i \quad k = 1, 2, \ldots, n^i \tag{27}$$

where P_k^i is the modal displacement, ω_k is the natural frequency of mode k, Q_k^i is the modal force associated with mode k, and n^i is the number of modes of the track link i. The modal force Q_k^i is a nonlinear function of time because it includes the effect of the inertia, contact, and joint forces acting on the track link i. The solution of the preceding equation is given by

$$P_k^i(t) = P_{k0}^i \cos(\omega_k t) + \frac{\dot{P}_{k0}^i}{\omega_k} \sin(\omega_k t) + \frac{1}{\omega_k} \int_0^t Q_k^i(\tau) \sin \omega_k (t - \tau)\, d\tau \tag{28}$$

where P_{k0}^i and $\dot{P}_{k0}^i$ are the initial conditions associated with the kth modal displacement and velocity, respectively. The last term of equation (28) is called the Duhamel or convolution integral, which is evaluated numerically in this investigation using Simpson's rule.

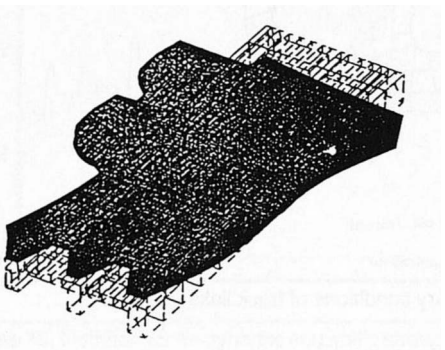

mode 1 600.27 Hz

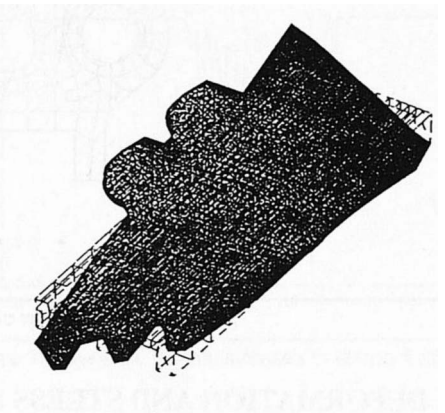

mode 4 876.94 Hz

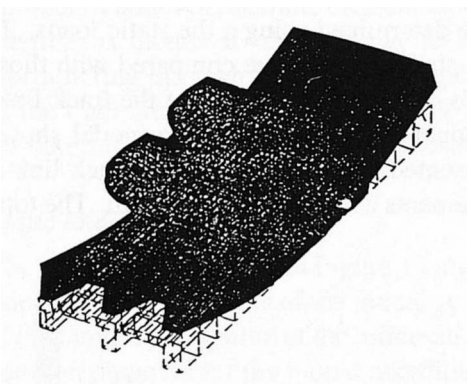

mode 2 633.47 Hz

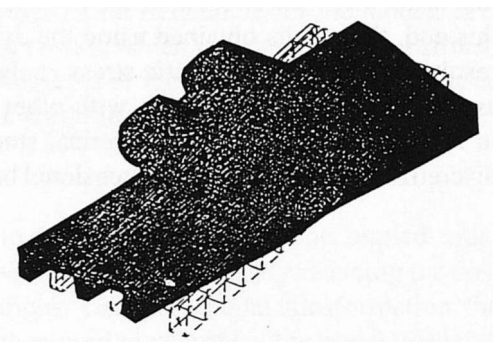

mode 5 1439.16 Hz

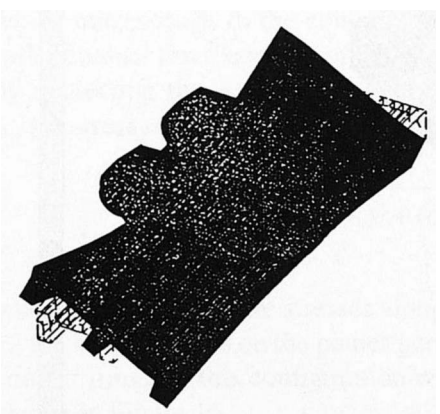

mode 3 875.96 Hz

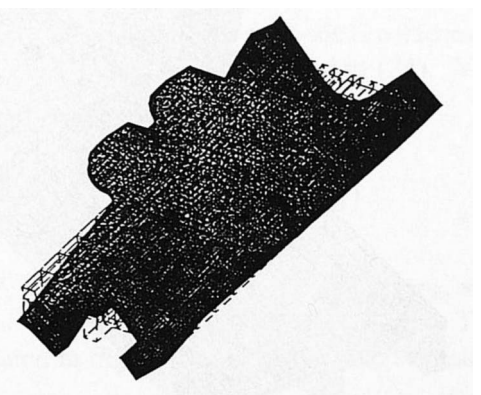

mode 6 1726.65 Hz

Figure 13. Mode shapes.

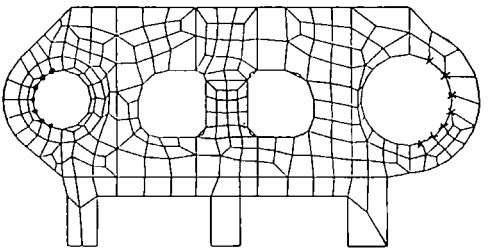

Figure 14. Planar view of the boundary conditions of track links.

7. DEFORMATION AND STRESS RESULTS

One of the main objectives of this study is to demonstrate the discrepancies and errors that arise when the stresses of the track links are determined using a the static loads. To this end, the results obtained using the dynamic stress analysis are compared with those results obtained using a static stress analysis. To examine the stresses of the track links as the result of its interaction with other components of the system, the model shown in Figure 1b is used in the numerical study presented in this section. The track link is discretized into 1,030 three-dimensional brick elements as shown in Figure 12b. The total

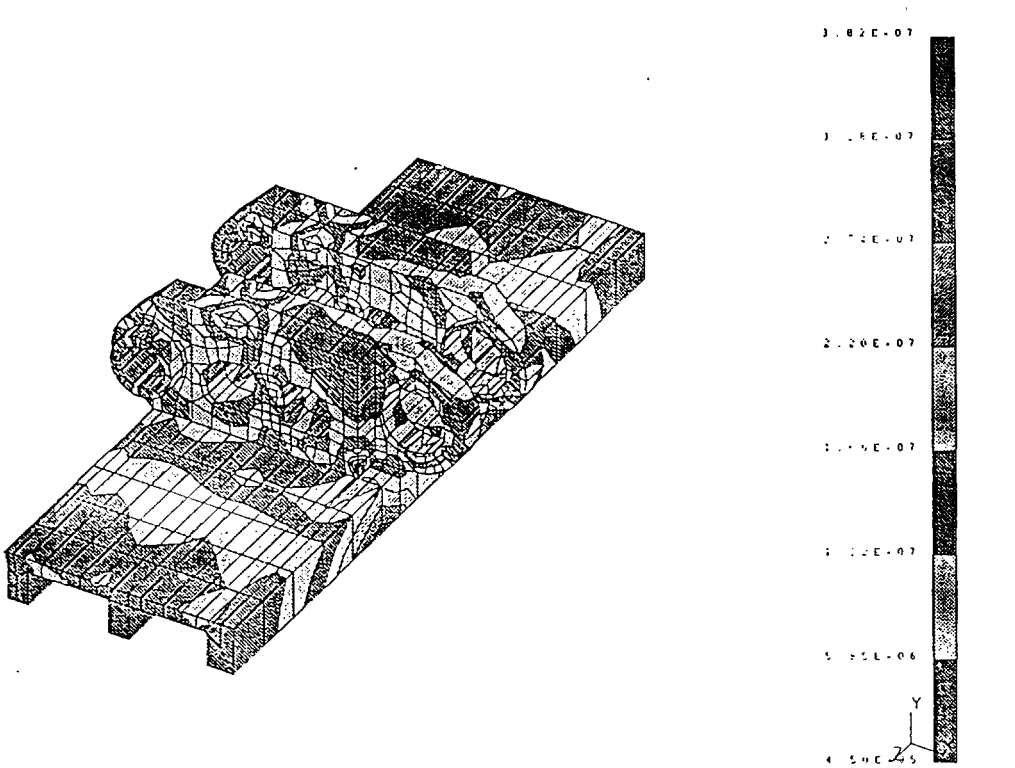

Figure 15. Von Mises stress distribution as the result of the static loads at time t = 3.6 s.

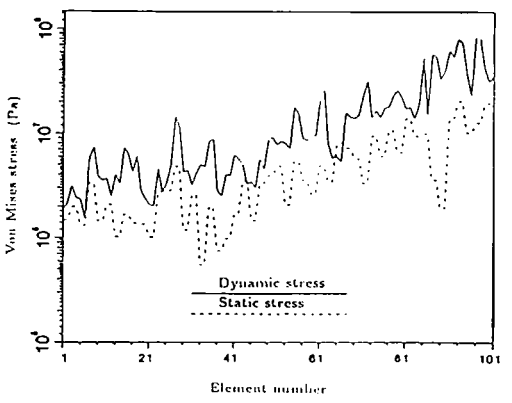

Figure 16. Comparison of dynamic and static stresses at time t = 3.6 s.

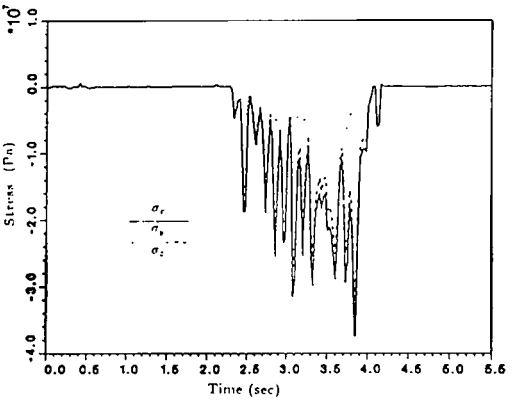

Figure 17. Dynamic normal stresses of element 361.

number of nodes of the finite element model shown in this figure is 2,046. Figure 13 shows the first six modes of vibration and the associated natural frequencies of the model. It is worth noting the high natural frequencies of the model, which indicate the high stiffness of the track links. Figure 14 shows the end conditions or the boundary constraints used for determining the natural frequencies and link mode shapes shown in Figure 13.

Static and Dynamic Stresses

The mode shapes shown in Figure 13 are used to obtain a reduced set of decoupled equations expressed in terms of the modal coordinates, thereby substantially reducing the cost of the numerical solution of the differential equations. Using the modal transformation, the solution obtained for the modal coordinates is then used to determine the nodal displacements, which are used to calculate the stresses in the track links (Pachner, 1984; Reddy, 1984). Furthermore, the static stress (Von Mises) is also determined at time t = 3.6 s, which corresponds to the configuration at which the track link experiences a maximum roller contact force because of the gravity effect of the vehicle. The analysis is performed by neglecting the terms $\mathbf{m}_{ff}^{i}\ddot{\mathbf{q}}_{f}^{i}$ in equation (23), $(\mathbf{Q}_{v}^{i})_{f}$ and $\mathbf{m}_{fr}^{i}\ddot{\mathbf{q}}_{r}^{i}$ in equation (24). Von Mises stress σ_v is defined as (Cook and Young, 1985)

$$\sigma_v = \frac{1}{\sqrt{2}}\sqrt{(\sigma_x - \sigma_y)^2 + (\sigma_y - \sigma_z)^2 + (\sigma_z - \sigma_x)^2 + 6\left(\tau_{xy}^2 + \tau_{yz}^2 + \tau_{zx}^2\right)}$$

where σ_x, σ_y, and σ_z are stresses along the X, Y, and Z axes, respectively, and τ_{xy}, τ_{yz}, and τ_{zx} are shear stresses on the planes perpendicular to the X, Y, and Z axes, respectively. The contact forces at this configuration were presented in Figure 10, while the static stress is shown in Figure 15.

In evaluating the dynamic stresses, the effect of all the forces acting on the track link is taken into consideration by first defining the modal forces and then using these forces in the Duhamel integral, which is evaluated numerically. Figure 16 compares the static stress due to the forces that act on the track link at time t = 3.6 s and the dynamic stress computed by taking into consideration the force history. It is clear from the results presented in this

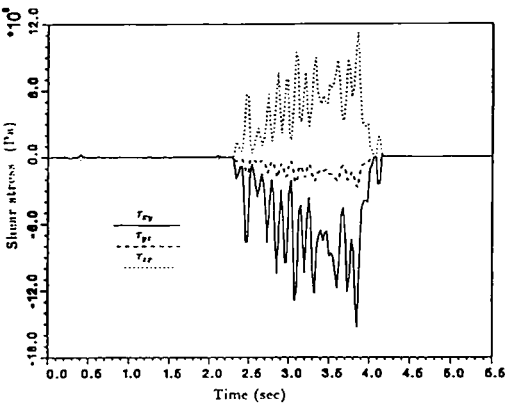

Figure 18. Dynamic shear stresses of element 361.

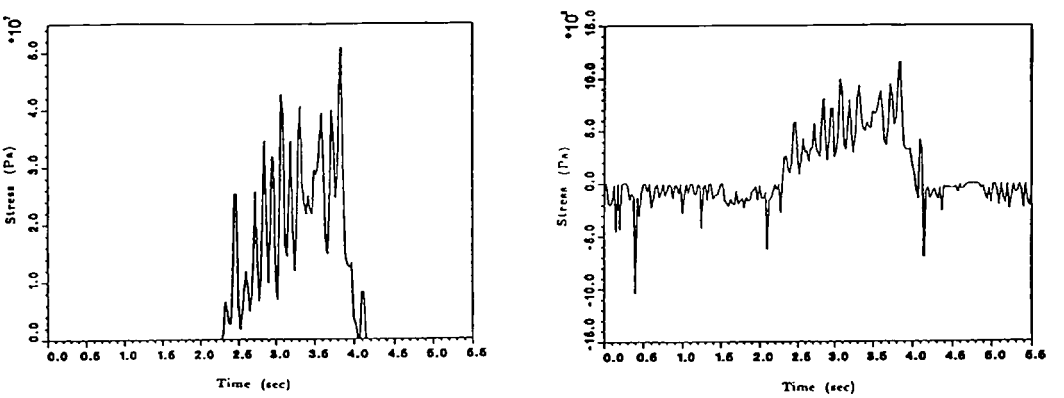

(a) Maximum principal stress (b) Minimum principal stress

Figure 19. Dynamic maximum and minimum principal stresses of element 361.

figure that there are significant differences that indicate that the use of the static stress analysis is not a conservative approach for the stress analysis and design of the track links.

Stress Time History

To examine the stress level of the chain links during a complete cycle of rotation of the track, we consider one element (element number 361) on the track link. This element is located on the top surface of a link that comes in direct contact with the rollers as shown in Figure 12b. Figure 17 shows the normal stresses due to the forces acting on the link. The results presented in this figure show that the maximum stress σ_x occurs when the track links are in contact with the ground and these stresses are primarily due to bending resulting from the dominant roller contact force. The results presented in this figure show that the stress σ_y is mainly compressive as the result of the ground reaction forces, which is also the case for the stress σ_z. Figure 18 shows the shear stresses τ_{xy}, τ_{yz}, and τ_{zx}. The results presented in this figure show that among these stresses, τ_{xy} has the most significant effect on the element, while τ_{yz} has the least effect. The maximum and minimum principal stresses acting on element 361 are shown in Figure 19. The maximum contribution to

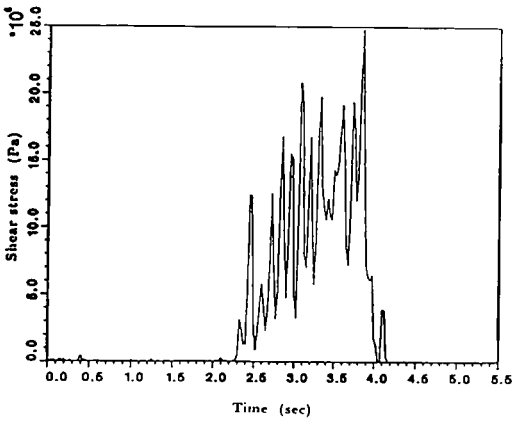

Figure 20. Dynamic maximum shear stress (τ_{max}) of element 361.

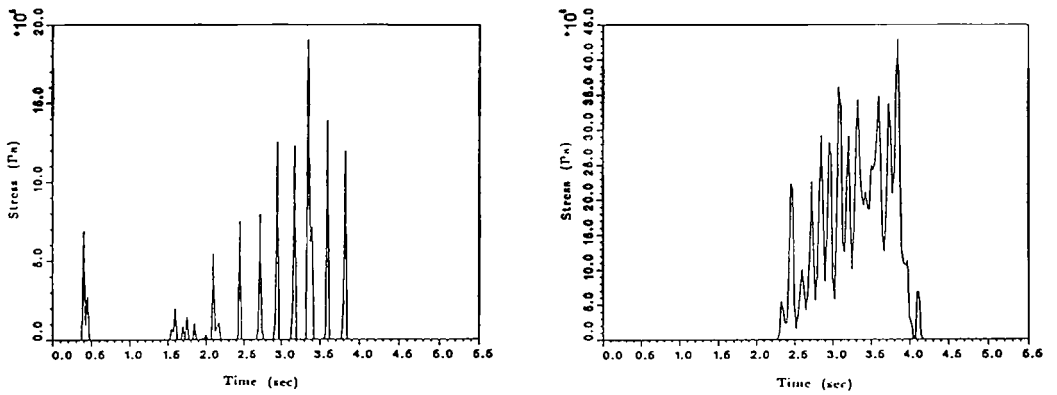

Figure 21. Dynamic Von Mises stresses of element 361 due to the separate effects of (a) the roller contact and (b) the ground contact forces.

this maximum principal stress comes from the interaction between the track links and the rollers. The maximum shear stress τ_{max} is shown in Figure 20.

Separate Effect of the Individual Forces

Despite the fact that the forces acting on a track link cannot, in general, be treated independently, we examine in this investigation the contribution of individual force components to the dynamic stresses of the track links. Figure 21 shows the Von Mises stress of the element 361 as the result of the separate effects of the roller and ground contact force. The discontinuity of the roller contact force stress shown in this figure clearly demonstrates the nature of the link roller contact during a complete cycle of the track, while the continuity of the stress due to the ground contact force is apparent. Figure 22 shows the stresses in the element as the result of the separate effects of the joint reaction forces, the sprocket driving forces, and the inertia forces. At the starting time of the track link cycle, the stress

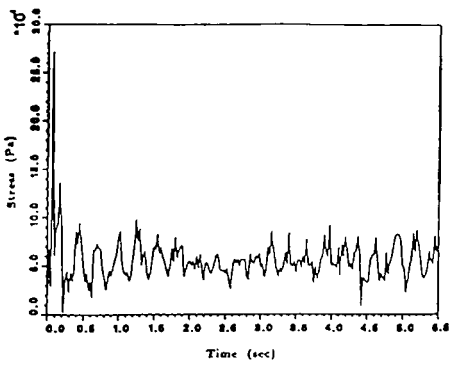

(a) Effect of joint reaction forces

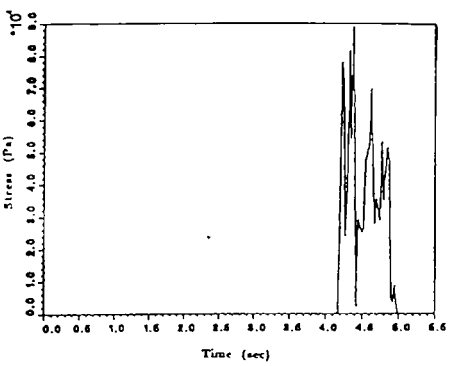

(b) Effect of sprocket driving forces

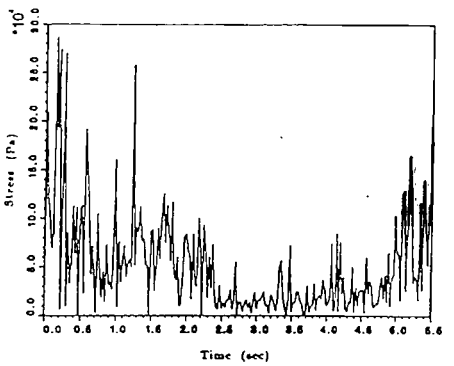

(c) Effect of inertia forces

Figure 22. Dynamic Von Mises stresses of element 361 due to the separate effects of the joint reaction, sprocket driving, and inertia forces.

due to the joint reaction forces attains a very high magnitude that dies out soon, leaving small fluctuations until the end of the cycle. It is also clear from the results presented in this figure that the dynamic stress caused by the sprocket driving force and the centrifugal inertia force is not significant as compared to the roller and ground contact forces.

8. SUMMARY AND CONCLUSIONS

In the analysis and design of tracked vehicles, the deformations of the track links are often analyzed using the methods of static stress analysis. The contribution and effect of each dynamic force such as the contact, inertia, centrifugal, and joint forces have not been

previously examined or quantified. The purpose of this investigation is to analyze the forces that act on the track links of multibody tracked vehicles and clearly demonstrate the inadequacy of using the methods of the static stress analysis in the deformation analysis of the track links. The equations of motion of the vehicle are obtained using the principle of virtual work in dynamics. The formulation leads to a set of nonlinear equations expressed in terms of coupled sets of reference and elastic coordinates. In the analysis presented in this paper, it is assumed that the deformation of the steel track links does not have a significant effect on the rigid-body motion of the tracked vehicle. A 54-body tracked-vehicle model is used in this study, and the track is modeled as closed chain that consists of 42 bodies connected by revolute joints. The pitch of the track chain used in the vehicle examined in this study is twice the pitch of the sprocket. Continuous force models are used to describe the interaction between the track links and the rollers, the idler, and the sprocket of the vehicle as well as the ground. The stiffness and damping coefficients used in these force models are obtained based on experimental observations (Nakanishi and Shabana, 1992, 1994). The global positions of the contact surfaces are monitored in order to be able to describe the interaction between the vehicle components. The model developed in this investigation, which includes significant details, is used to obtain the inertia, constraint, and contact forces that act on the track links during the complete cycle. These forces are used in a detailed stress analysis of the track links. The results of this analysis indicate that the dynamic stresses can be significantly different from those stresses determined using static forces. The most dominant forces that cause high stresses are the track-roller and track-ground contact forces, while the least significant forces were found to be the sprocket-track contact, and centrifugal inertia forces of the track links.

Acknowledgment. This work was supported, in part, by the U.S. Army Research Office, Research Triangle Park, NC.

REFERENCES

Bando, K., Yoshida, K., and Hori, K., 1991, "The development of the rubber track for small size bulldozers," International Off-Highway Powerplants Congress and Exposition, September 9–12, Milwaukee, WI.

Bucknor, N. K. and Freudenstein, F., 1992, "Kinematic and static force analysis of rocker-pin jointed silent chains with involute sprockets," Proceedings of the ASME 1992 Mechanisms Conference, DE-Vol. 46, September 13–17, Scottsdale, AZ.

Burnett, D. S., 1987, *Finite Element Analysis, From Concepts to Applications*, Addison-Wesley Publishing Co., Reading, MA.

Chen, D. C., Shabana, A. A., and Rismantab-Sany, J., 1991, "Generalized and actual constraint forces in the inverse dynamic analysis of spatial flexible mechanical systems," Proceedings of the ASME 1991 Design Automation, September 13–16, Miami, FL.

Chew, M., 1985, "Inertia effects of a roller-chain on impact intensity," *ASME Journal of Mechanisms, Transmissions, and Automation in Design* **107**, 123–130.

Cook, R. D. and Young, W. C., 1985, *Advanced Mechanics of Materials*, Macmillan Publishing Company, New York.

Khulief, Y. A. and Shabana, A. A., 1987, "A continuous force model for the impact analysis of flexible multibody systems," *Mechanism and Machine Theory* **22**(3), 213–224.

McCullough, M. K. and Haug, E. J., 1985, "Dynamics of high mobility track vehicle," *ASME Paper No-85-DET-95*.

Murray, M. and Canfield, T. R., 1992, "Modeling of a flexible link power transmission system," Proceedings of the 6th ASME International Power Transmission and Gearing Conference, September 13–16, Scottsdale, AZ.

Naji, M. R. and Marshek, K. M., 1983, "Experimental determination of the roller chain load distribution," *ASME Journal of Mechanisms, Transmissions, and Automation in Design* **105**, 331–338.

Naji, M. R. and Marshek, K. M., 1984, "Analysis of roller chain sprocket pressure angles," *Mechanism and Machine Theory* **19**(2), 197–203.

Nakanishi, T. and Shabana, A. A., 1992, "Dynamics of tracked vehicles," *Technical Report KMTR-92-001*, Department of Mechanical Engineering, University of Illinois at Chicago.

Nakanishi, T. and Shabana, A. A., 1994, "Contact forces in the nonlinear dynamic analysis of tracked vehicles," *The International Journal for Numerical Methods in Engineering* **37**, 1251–1275.

Pachner, J., 1984, *Handbook of Numerical Analysis Applications*, McGraw-Hill Book Publishing Co., New York.

Reddy, J. N., 1984, *An Introduction to the Finite Element Method*, McGraw-Hill Book Publishing Co., New York.

Shabana, A. A., 1989, *Dynamics of Multibody Systems*, John Wiley & Sons, New York.

Shabana, A. A., 1991, *Theory of Vibration, Volume II: Discrete and Continuous Systems*, Springer-Verlag, New York.

Shabana, A. A., 1994, *Computational Dynamics*, John Wiley & Sons, New York.

Veikos, N. M. and Freudenstein, F., 1992, "On the dynamic analysis of roller chain drives, parts I and II," Proceedings of the 1992 Mechanisms Conference, DE-Vol. 46, September 13–16, Scottsdale, AZ.

Wehage, R. A., 1980, "Generalized coordinate partitioning in dynamic analysis of mechanical systems," Ph.D. thesis, the University of Iowa, Iowa City.